Proceedings of the 2007 International Manufacturing Science And Engineering Conference
MSEC2007
October 15-17, 2007, Atlanta, Georgia, USA

MSEC2007-31155

GRAIN BOUNDARY RESPONSE OF ALUMINUM BICRYSTAL UNDER MICRO SCALE LASER SHOCK PEENING

Sinisa Vukelic
Mechanical Engineering Department
Columbia University in the City of New York
sv2147@columbia.edu

Jeffrey W. Kysar
Mechanical Engineering Department
Columbia University in the City of New York
jk2079@columbia.edu

Y. Lawrence Yao
Mechanical Engineering Department
Columbia University in the City of New York
yly1@columbia.edu

ABSTRACT

Micro scale laser shock peening (μLSP) is a process in which compressive residual stresses are induced in a material surface to improve fatigue life and wear resistance under cyclic loading. Since the diameter of the laser spot used during the process is the same order of magnitude as grain size, the effects of anisotropy and heterogeneity have to be explicitly taken into account. In this study experimental and analytic work have been done in order to investigate the bicrystal aluminum response under Gaussian loading. Effects of heterogeneity under μLSP are studied through applying laser shocks onto the grain boundary of the aluminum bicrystal. μLSP on reference single crystals have also been performed for the purpose of comparison. The orientations of the crystals in the bicrystal as well as the reference single crystals have been chosen such that an approximate plane strain condition is achieved. A finite element model has also been developed based on single crystal micromechanics and a cohesive zone interface model. Simulation results are compared with experimental findings. The potential benefit of μLSP as a surface treatment for improvement of fatigue life is also discussed.

INTRODUCTION

Laser shock peening (LSP) as a process of surface improvement (Clauer and Hoolbrook, 1981, Clauer and Lahrman, 2001) was introduced in 1960s as a potential replacement for conventional shot peening (Curtis et al., 2002). Both LSP and conventional shot peening induce compressive residual stresses of the same order of magnitude which improve material properties of various metals such as copper, nickel, aluminum, etc. (Hammersley, 2000) under cyclic loading. However, the use of laser shocking instead of bombarding a

surface with hard particles has a number of advantages. These advantages include deeper shock wave penetration as well as a significant increase in process flexibility with respect to the potential geometries of treated areas. On the other hand, the high cost of lasers powerful enough to produce beam spot size in the order of millimeters with power densities of several GW/cm^2 has prevented wider industry application of LSP.

The development of micron size devices like micro electromechanical systems (MEMS), micro switches, etc. has raised the issue of improvement of reliability of these components. In order to improve its fatigue life and wear resistance micro scale laser shock peening (μLSP) has been developed (Zhang and Yao, 2002) which employs laser beam spot size of approximately 10 microns. The surface of interest is coated with thin aluminum foil or paint to protect the surface from thermal effects and thus to prevent change in microstructure due to high temperatures. The upper portion of coating is ablated creating plasma which induces a pressure shock and mechanically alters residual stress distribution (Chen et al., 2004). At first, most of the studies involved polycrystalline materials (Zhang and Yao, 2002.). However, because of the fact that beam diameter size is in the same order of magnitude as the average size of grains in aluminum and copper, the materials must be treated as being anisotropic and inhomogeneous, which motivates the current line of research. The study of anisotropy has been performed using single crystals under μLSP of aluminum and copper by Chen et al. (2004) and Wang et al. (2005) utilizing anisotropic slip line theory. In order to further understand the effect of anisotropy, the response of two different orientations of single crystal aluminum are compared (Vukelic et al., 2006) to analyze the difference between single and double slip case.

The grain size plays a very important role in the mechanical behavior of polycrystalline metals. Therefore it is of interest to investigate interaction between grains. First to set dependence between size of the grain and yield stress were Hall (1951) and Petch (1953), producing Hall-Petch relation. The grain boundary serves as an obstacle to the motion of dislocations causing them to pile up at the boundary resulting in a stress concentration. Livingston and Chalmers (1957) employed isoaxial aluminum bicrystals to study the process of secondary slip activation. Heterogeneity was further analyzed by Rey and Zaoui (1979) who considered geometrical aspects of slip heterogeneities in aluminum bicrystals and made comparison with the single crystal response. These studies were predominantly experimental and involved tensile tests and examination of free surfaces. Hook and Hirth (1967) examined Fe-3%Si alloy bicrystals to investigate the influence of plastic and elastic incompatibility on stress concentrations at the grain boundary. Their study involved analysis of dislocation structure in the interior.

More recent studies focused on fundamental aspects of grain boundary interactions. Mesarovic and Kysar (1996) analyzed dislocation nucleation and crack growth at the boundary of Cu/Al_2O_3 bicrystals. They described the crack tip stress field under static loading with plane strain conditions, by analytical derivation and conducted numerical investigation using 'small strain', finite deformation and ideal plasticity formulations. Kysar (2000) analyzed further the directional crack growth dependence at the interface of a copper/sapphire bicrystal. The investigation included finite element analysis and experimental results with extensive review of single crystal plasticity. Evers et al. (2002) developed a model which divides grain into two parts a core and several bicrystal boundaries. In that work it is stated that heterogeneous deformation between core and boundaries initiates the formation of geometrically necessary dislocations (GNDs) to maintain lattice compatibility. Furthermore according to this approach newly created GNDs prevent dislocation motion which results in enhanced hardening. This work is mainly analytical. Another model based on GNDs is proposed by Ma et al. (2006). This study examines interaction between dislocations and grain boundaries from the theoretical and experimental point of view under a simple shear test. Wei and Anand (2004) discussed the effects of grain boundary sliding and separation in polycrystalline nickel. They coupled a single crystal plasticity model for grain interior with an elastic-plastic grain boundary interface model. Moreover they developed a numerical model for a qualitative study of deformation and fracture response of nanocrystalline nickel in simple tension.

The purpose of the present study is to examine the effect of heterogeneity under μLSP through numerical and experimental work. Therefore, a finite element model will be developed to investigate the aluminum bicrystal response

under Gaussian pressure loading and series of experiments are conducted for comparison. The benefit of μLSP as a surface treatment for improvement of fatigue life will also be discussed.

EXPERIMENTAL SETUP

SAMPLE PREPARATION

In this study an aluminum bicrystal grown from the melt was used. It was mounted on a three circle goniometer and the orientations of its crystals were determined using Laue diffraction to within ±1º. It is a tilt-type grain boundary with the [110] direction in both crystals parallel to the tilt axis of the adjoining grains, as seen on Figure 1.

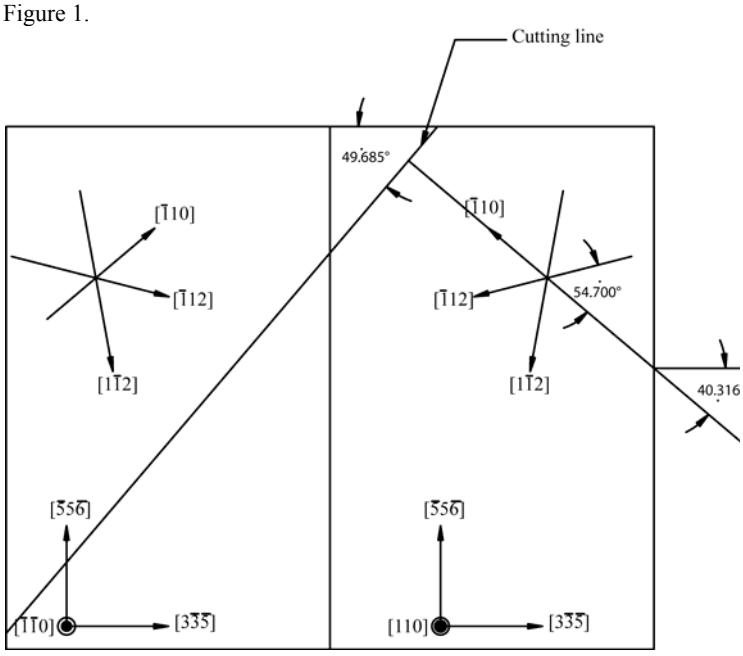

Figure 1: Bicrystal orientation prior cutting

This was done to ensure approximate plane strain deformation in both crystals after laser shocks are applied along the grain boundary. The specimen was cut from the as-grown bicrystal using a wire electro-discharge machine (EDM) to 46 mm long, 11.6 mm wide and 7.7 mm high. The surfaces of the individual crystals to be shocked deviated about 9.5º and 2.5º, respectively from the ideal (110) and (001) surfaces. The sample was later mechanically polished in order to remove the heat affected zone (HAZ), followed by electropolishing to remove any remaining residually stressed material. The bicrystal was afterwards etched with a solution of sodium hydroxide and deionized water for about two minutes to reveal the grain boundary along which laser shocks were to be applied. After shocking and subsequent characterization of the top surface were completed, the specimen was sectioned using the EDM in order to examine the cross section. The same polishing procedure was then applied to the cross section.

SHOCKING

A frequency tripled Q-switched Nd:YAG laser with wavelength λ = 355 nm in TEM_{00} mode is used for the μLSP experiments. The beam diameter is 12 μm and pulse duration is 50 ns with approximate laser energy of 320 μJ. The specimen was placed in a shallow container mounted on a computer controlled Aerotech motorized linear stage where the laser beam path was carefully aligned with the grain boundary. Since the diameter of the laser beam is four orders of magnitude larger than the width of the grain boundary it is expected that laser shock were placed either on the boundary or very close to it along the entire shock line. After alignment, a thin layer of vacuum grease was spread on the top surface and a 16 micron thick polycrystalline aluminum foil was applied in order to prevent thermal effects from reaching the surface of the bicrystal. The container was then filled with distilled water which was used as a confining medium and laser shocks were applied with 25 μm spacing. The overall experimental setup is illustrated in Figure 2. A similar procedure was followed for shocking reference single crystals away from the grain boundary. More details about laser shocking can be found at Zhang and Yao (2000), Chen et al. (2004), Wang et al. (2005) and Vukelic et al. (2006). Two dimensional deformation is achieved by applying load along the (110) direction in FCC crystals is discussed in Rice (1972 and 1987), Kysar et al. (2004), Crone et al. (2004), Wang et al. (2005), and Vukelic et al. (2006).

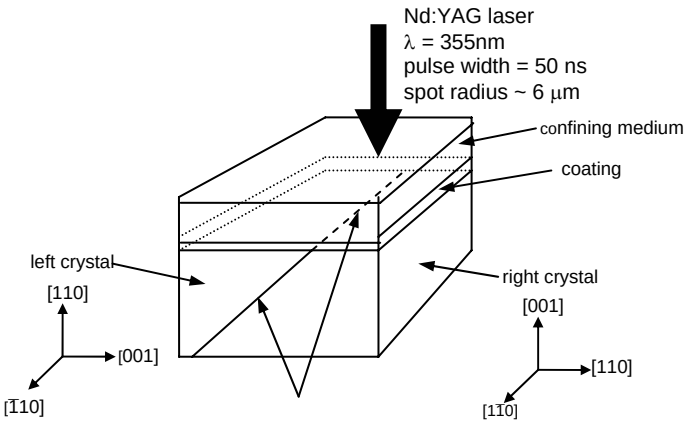

Figure 2: Experimental setup

CHARACTERIZATION

Prior to shock peening, the surface roughness of the sample was measured using an atomic force microscope (AFM), in order to establish the baseline roughness and determine influence of etching on the bicrystal grain boundary. After shocking, the geometry of the affected region was characterized using a profilometer. In addition, the size of the plastically deformed region was estimated by characterizing the region over which significant crystal lattice rotation occurred (Kysar and Briant, 2002, Wang et al., 2005, Vukelic et al., 2006). For this purpose Electron Backscatter Diffraction (EBSD) was employed to spatially map the crystallographic orientation as a function of position along the shocked surface using a JEOL JSM 5600LV scanning electron microscope with HKL Technology EBSD system. Crystallographic orientations were determined over regions with extents of 190 μm x 285 μm and 120 μm x 240 μm on the top surface and cross section, respectively. A similar procedure carried out for characterizing the reference single crystals.

CONSTITUTIVE MODEL

The bicrystal model developed in this work is decomposed into the single crystal interior and grain boundary. In the work presented here we use the crystal plasticity theory developed by Hill (1950), Rice (1973, 1987), Asaro (1983) and Asaro and Needleman (1985). According to this theory plastic deformation occurs on slip systems described by slip directions and slip normals. Micromechanics of single crystals is applied to the grain interiors. The grain boundary will be modeled by implementing a cohesive zone model that takes into account interactions at the boundary of the bicrystal by describing sliding and debonding.

COHESIVE ZONE MODEL

Cohesive surface models were introduced in the mid 20th century by early work of Barenblatt (1959) to describe crack propagation. Further development and numerical implementation has been done by Needleman (1987) and Xu and Needleman (1993, 1994) who used a cohesive surface separation law to predict the propagation of fracture. Wei and Anand (2004) adopted similar approach to simulate sliding and separation between grains in nanocrystaline nickel. The following paragraphs summarize the constitutive relations to be used to describe interactions at a grain boundary of an fcc bicrystal.

The surface traction across the cohesive zone can be expressed in terms of a potential function in the following form

$$T = \frac{\partial \phi}{\partial \Delta} \tag{1}$$

Where ϕ is the potential function and Δ is the separation of the two adjoined surfaces. The potential suggested by Xu and Needleman (1993) allows for both tangential and normal debonding:

$$\phi(\Delta) = \phi_n + \phi_n \exp\left(-\frac{\Delta_n}{\delta_n}\right)\left\{\left[1 - r + \frac{\Delta_n}{\delta_n}\right]\frac{1-q}{r-1} - \left[q + \left(\frac{r-q}{r-1}\right)\frac{\Delta_n}{\delta_n}\right]\exp\left(-\frac{\Delta_t^2}{\delta_t^2}\right)\right\} \tag{2}$$

where the subscripts *n* and *t* indicate normal and tangential quantities, respectively. Further, the quantities

$$q = \frac{\phi_t}{\phi_n}, r = \frac{\Delta_n^*}{\delta_n} \tag{3}$$

can be defined where Δ^* represents the magnitude of discontinuity after separation is complete and no tractions left. In addition, Φ_t and Φ_n are the work of tangential and normal separation, respectively while δ_t and δ_n are the characteristic tangential and normal length scales, respectively. This leads to the following relations for surface tractions in the tangential and normal directions.

$$T_n = -\frac{\phi_n}{\delta_n}\exp\left(-\frac{\Delta_n}{\delta_n}\right)\left\{\frac{\Delta_n}{\delta_n}\exp\left(-\frac{\Delta_t^2}{\delta_t^2}\right) + \frac{1-q}{r-1}\left[1 - \exp\left(\frac{\Delta_t^2}{\delta_t^2}\right)\right]\left[r - \frac{\Delta_n}{\delta_n}\right]\right\} \tag{3}$$

$$T_t = -\frac{\phi_n}{\delta_n}\left(2\frac{\delta_n}{\delta_t}\right)\frac{\Delta_t}{\delta_t}\left\{q + \left(\frac{r-q}{r-1}\right)\frac{\Delta_n}{\delta_n}\right\}\exp\left(-\frac{\Delta_n}{\delta_n}\right)\exp\left(-\frac{\Delta_t^2}{\delta_t^2}\right)$$

SINGLE CRYSTAL PLASTICITY

The single crystal plasticity theory assumes that the deformation gradient tensor can be multiplicatively decomposed into two components, one responsible for plastic shear and other for elastic stretching and lattice rotation, as illustrated at Fig. 3. In this way all the effects of finite deformation can be incorporated into the theory.

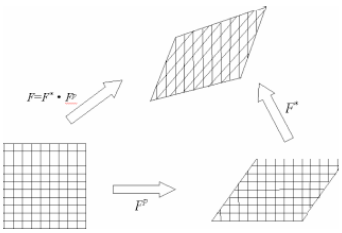

Figure 3: Single crystal plasticity – lattice rotation and slip

NUMERICAL IMPLEMENTATION

The commercial finite element code ABAQUS/standard is used for numerical simulations, accompanied by user defined subroutines, UMAT, written by Huang (1991) and modified by Kysar (1997) and user defined element (UEL) subroutine written by Becker (1988) and modified by Kysar (1999). The cohesive zone UEL allows both debonding and slip to occur between two surfaces, in this case the grain boundaries of the adjacent crystals. The model is quasi static and two dimensional. Boundary conditions are set on the bottom to be zero displacement. A Gaussian pressure loading is applied on the top surface at the grain boundary interface.

The finite element mesh model is shown in Figure 4 and was created such that all elements within the grain interior are quadrilateral while preserving specific angle between grains. For the grain interior 4-node quadrilaterals elements were used which have a 'hybrid' formulation with selectively reduced integration (ABAQUS/Standard User's Manual, 2001). The material properties chosen were appropriate for aluminum and they are incorporated within UMAT. At the grain boundary the UEL which used the Needleman and Xu (1994) potential described in detail in previous section. was employed. The parameters employed in the UEL effectively define the threshold for debonding under the given loading conditions. Parameters are characteristic normal and tangential displacement $\delta_t = \delta_n$ = 2.45e-6; maximum normal stress σ_{max} = 450 MPa, normal shear coupling parameter q = 1.

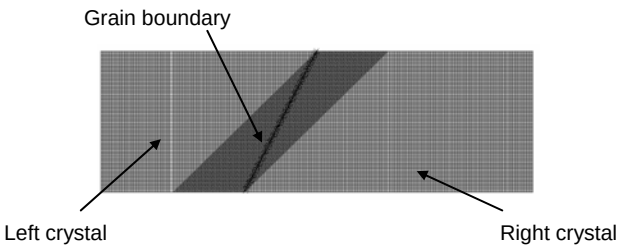

Figure 4: Mesh for finite element model

RESULTS AND DISCUSSION

GEOMETRY OF SHOCKED REGION

The geometry of the surface prior to and after shocking was measured using an atomic force microscope (AFM) and profilometer. Results of the AFM are shown in Figure 5. The specimen was etched using sodium hydroxide before shocking in order to see the grain boundary, so it is off interest to see if the chemical etched away a portion of the surface near the grain boundary that might affect the depth and shape of deformation. Figure 5c shows that the surface roughness does not exceed 100 nm and that no distinctive groove due to etching is formed at the grain boundary. Similar conclusions can be drawn for reference baselines in single crystals, shown on the Figures 5a and 5b. Figure 6 shows the geometric profile at the grain boundary from the profilometer measurements and in reference single crystals after shocking. Several measurements along the shock lines have been performed giving similar results, which indicate that deformation is to a good approximation two dimensional. From Figure 6 it can be observed that depth of deformation in both bicrystal and reference single crystal is about the same and on average it is approximately 80 μm. It can also be seen that the width of deformation is slightly wider at the grain boundary of the bicrystal than in the single crystals.

ELECTRON BACKSCATTER DIFFRACTION INVERSE POLE FIGURES

Laser shocks cause plastic deformation that can be characterized by the change in the local crystallographic orientation obtained via electron backscatter diffraction (EBSD) measurements. One method to present the results is with inverse pole figures of the crystallographic orientation over the area of interest. An inverse pole figure of the untreated bicrystal at the grain boundary is shown in Fig. 7. The shocked reference single crystals of (110) and (001) orientation as well as treated grain boundary is shown in Fig. 8. The results show a definite change in crystallographic orientation after treating with μLSP as a consequence of lattice rotation. We can also observe that the change in crystallographic orientation is larger in the (110) crystal than in the (001) which is consistent with lattice rotation measurements shown in the next section.

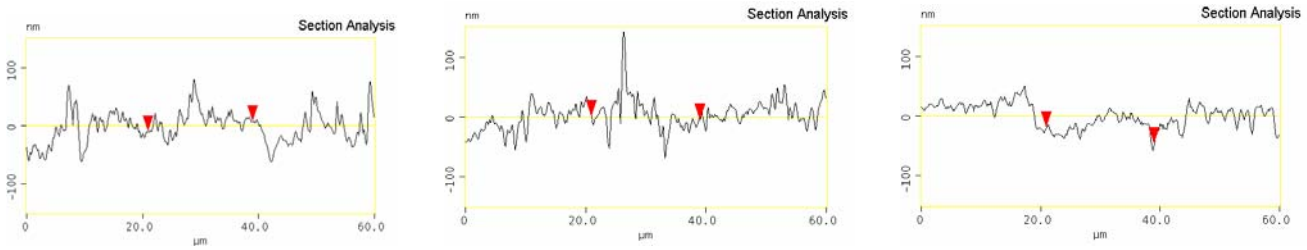

(a) **(b)** **(c)**

Figure 5: Surface roughness – AFM measurements prior shocking (a) single crystal (110) (b) single crystal (001) (c) grain boundary

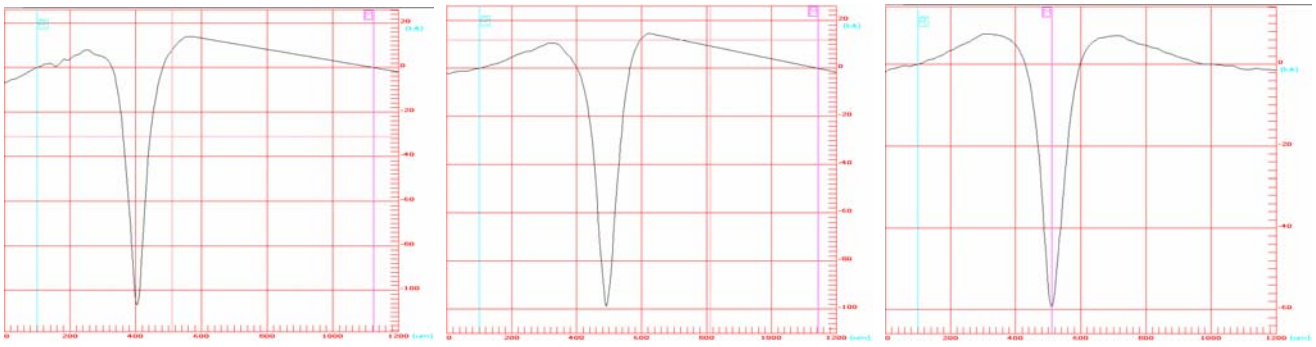

(a) **(b)** **(c)**

Figure 6: Deformation geometry after shocking (a) single crystal (110) (b) single crystal (001) (c) grain boundary

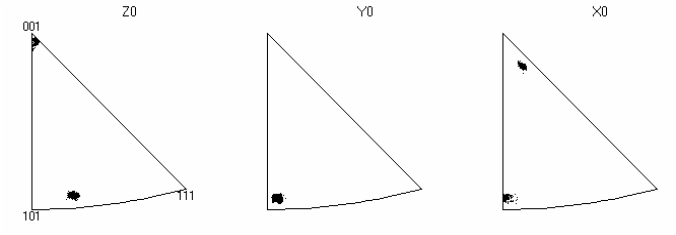

Figure 7: Untreated bicrystal inverse pole figure

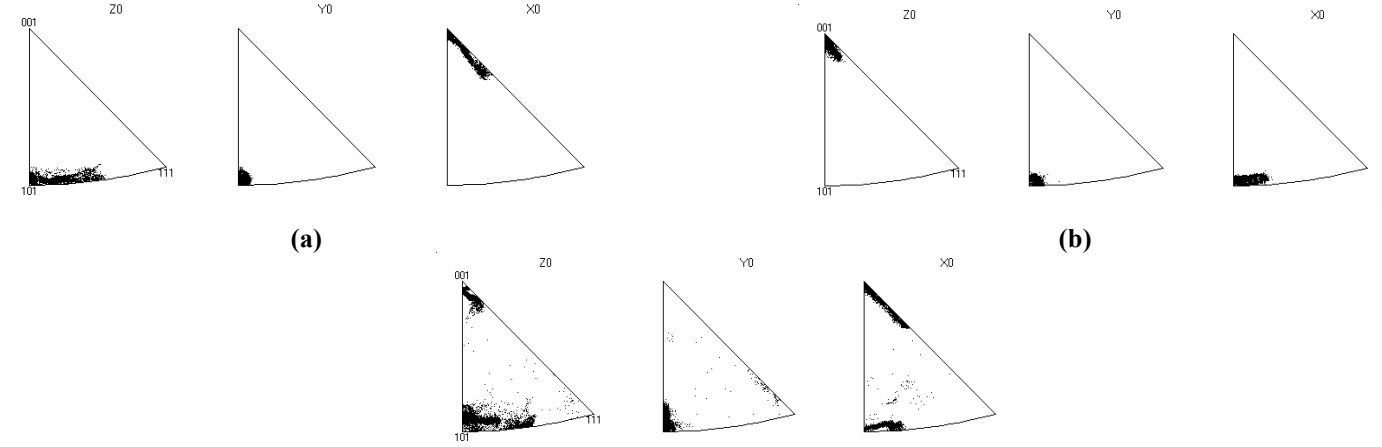

(a) **(b)**

(c)

Figure 8: Inverse pole figure after μLSP (a) single crystal (110) (b) single crystal (001) (c) grain boundary

LATTICE ROTATION OF TOP SURFACE

Mapping of the crystal lattice rotation on the shocked surface of the reference single crystals and near the grain boundary of the bicrystal are shown in Figure 9. Green regions represent rotation free regions whereas the regions rotated about the shock line (i.e. the y-axis) in the counter clockwise direction are blue and clockwise rotated area is red. Furthermore, for the bicrystal configuration, the clockwise rotation is associated with (110) crystal while counter clockwise rotation is in the (001) crystal. From Figure 9 it can be seen that deformation is fairly uniform along the shock line in both the bicrystal and reference single crystals indicating that approximate plane strain deformation states have been achieved. Deformation in the reference single crystal is, as expected, approximately symmetric because of the corresponding plastic yield loci corresponding to the (110) and (001) orientations (Rice, 1987, Kysar et al., 2004, Vukelic et al., 2006). The deformation width is about 150 μm and 140 μm in the (110) and (001) case, respectively. Rotation in the (110) crystal is between -9° and 9° and it is larger than the (001) where it ranges from -7° to 7°. Also it should be noted that the unrotated region where the shock line lies is much narrower for the (110) case than for the (001).The shocked, region near the grain boundary can be seen in Figure 9c.

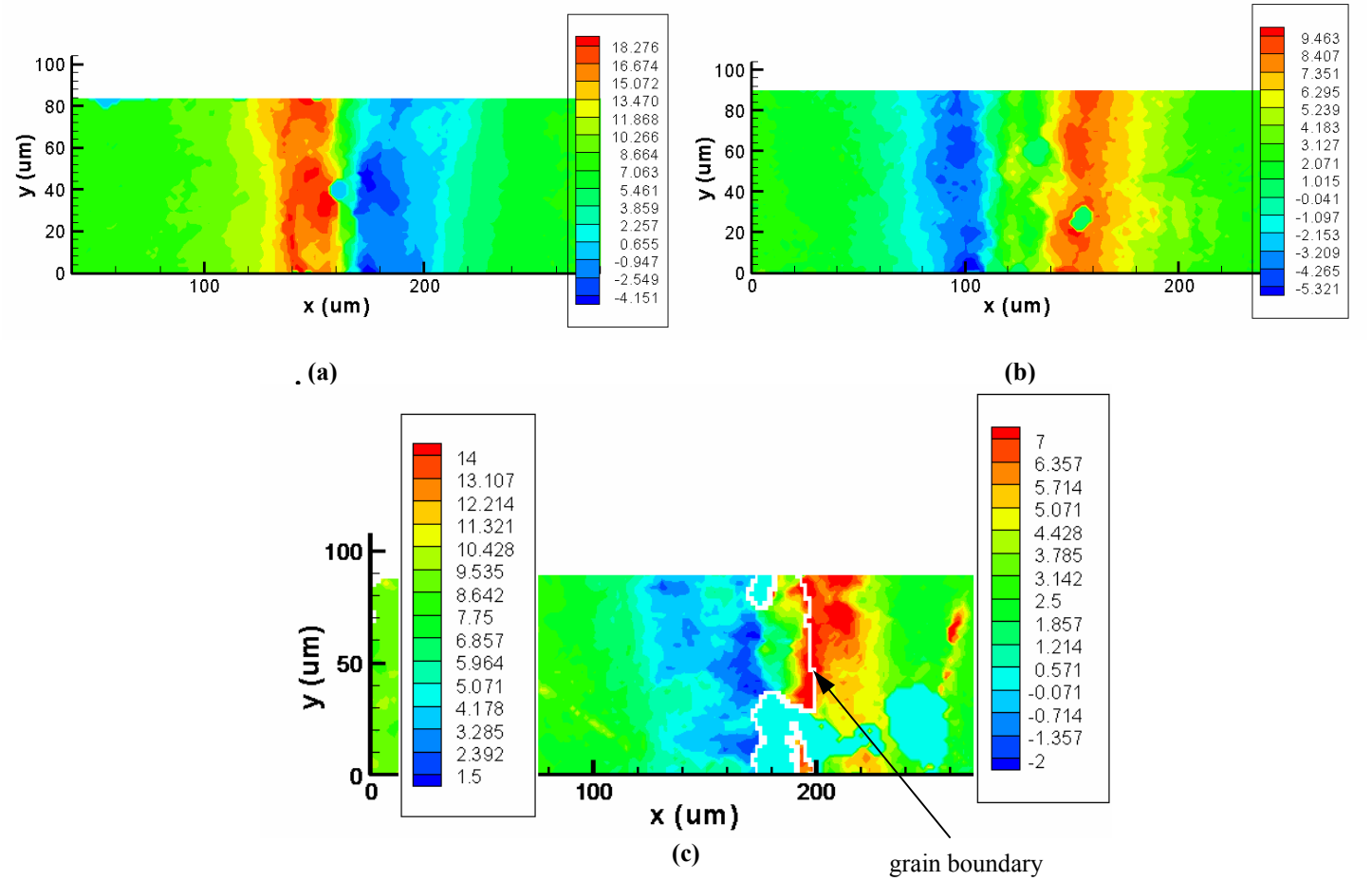

Figure 9: Lattice rotation at the top surface (a) single crystal (110) (b) single crystal (001) (c) grain boundary

Although the deformation appears similar to the single crystal references (110 and 001) suggesting the validity of the plane strain assumption, several differences should be noted. First, deformation is not symmetric with respect to the shock line. From Figure 9c it can be observed that the green region (zero rotation) in the middle of the affected area is shifted toward the left with respect to the grain boundary. That is due to the fact laser shocks were applied close to the grain boundary, but not exactly at the grain boundary. Thus, deformation in the (110) crystal contains clockwise, zero and some

counter clockwise rotation while for the (001) crystal there is only counter clockwise rotation. Second, the magnitude of rotation at the bicrystal grain boundary as compared to the reference single crystals is smaller. When we compare the (001) reference single crystal and (001) crystal of the bicrystal we can see that the rotation is about 2° smaller in the bicrystal. An even larger discrepancy can be observed in the (110) crystal where the difference is about 4°. Less deformation may arise in the bicrystal due to the fact that the grain boundary acts as an obstacle to the motion of dislocations and thus they pile up at it making the nearby region harder to deform. Lastly, a discontinuity in lattice rotation can be observed at the grain boundary. The magnitude of rotation adjacent to the grain boundary from the (110) crystal is about 14° and on the other side of the grain boundary is 7°. When we look at these values with respect to the reference crystal orientation mentioned in the paragraph above, the relative difference in lattice rotation across the grain boundary is approximately 1.5°.

LATTICE ROTATION OF CROSS-SECTION

Mapping of the cross section of the bicrystal and reference (001) single crystal was performed using electron backscatter rotation (EBSD) and the lattice rotation is calculated from those data with results shown in Figure 10. Results for cross sectional lattice rotation of the (110) crystal can be found at Vukelic et al. (2006) and Chen et al. (2004). From Fig. 10a it can be seen that the deformation width is approximately 160 μm which is consistent with top surface observations and depth is about 50 μm. The lattice rotation pattern agrees very well with the finite element model of single crystal μLSP done by Chen et al. (2004). The pattern is also symmetric which can be correlated with analytic solution for double slip case under μLSP, discussed in detail for the (110) orientation single crystal aluminum in Vukelic et al. (2006). Lattice rotation near the grain boundary is shown at Fig. 10b. Due to the backlash of stage used, laser shocks were offset approximately 70 μm from the grain boundary towards the (110) crystal interior, for the region chosen for the cross section characterization. Thus it appears that (001) crystal side of the grain boundary was not affected by the shocking. Figure 10b shows a deformation width of about 90 μm which might be even larger because information close to the sample surface is lost due to the edge rounding during electropolishing of the specimen. The same statement applies to the deformation depth which appears to be approximately 50 μm which is consistent with the reference single crystal results.

NUMERICAL RESULTS

LATTICE ROTATION

In the finite element analysis, loading is applied directly over the grain boundary of the two crystals so the grain boundary effect can be studied numerically. Loading follows a Gaussian distribution and it is given with:

$$P(x) = P_o \cdot \exp\left(-\frac{x^2}{2R^2}\right) \tag{4}$$

where R is the beam radius, x represents the distance from the center of the Gaussian pressure distribution. P_o is the peak pressure and it is put in the numerical model in non-dimensional form $P_o/\tau_{CRSS} = 7$. τ_{CRSS} represents critical shear strength at each slip system and it is approximately 1 MPa.

Numerical results for in plane crystallographic lattice rotation along the cross section can be seen at Figure 11. Results and

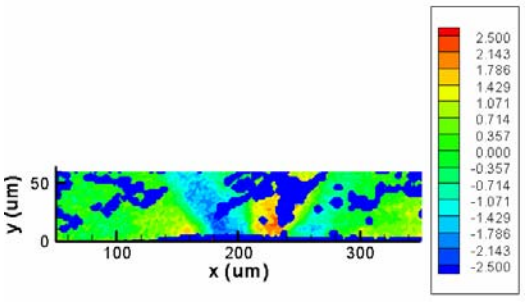

(a)

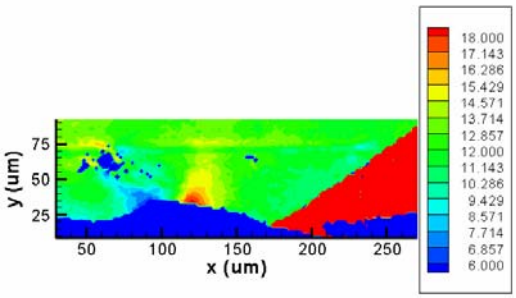

(b)

Figure 10: Lattice rotation – cross section (a) single crystal (001) (b) grain boundary

discussion for the reference single crystals of (110) and (001) orientation can be found in Chen et al. (2004) and Vukelic et al (2006), thus they will not be further elaborated upon here.

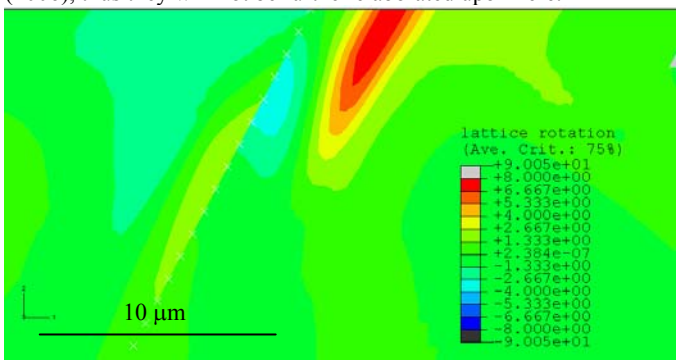

Figure 11: Numerical results – lattice rotation at grain boundary

The magnitude of maximum rotation is $\pm 7^{o}$ and the total deformation width is 38 μm and depth is 15 μm. The discrepancy between experimental and numerical results with respect to lattice rotation and deformation may be explained by the fact that the applied loading in the simulation is an order of magnitude lower than those of the experiments. The magnitude of the load applied in the simulation was treated as a free parameter and was previously adjusted in order to calibrate the numerically calculated displacements such that they match those observed experimentally. This was done as there is no direct means for matching the loads from an experimentally dynamic situation to that of the static simulation. It should be noted that the width of deformation in the left crystal is twice as large as the one in the right crystal. Also, although both crystallographic orientations have symmetric yield loci giving symmetric lattice rotation patterns in reference single crystals under Gaussian loading (Chen et al, 2004, Vukelic et al, 2006), the presence of the grain boundary plays a major role in case of the bicrystal. Non-symmetry of the domain of interest causes crystallographic lattice rotation to be non-symmetric as seen in Fig. 11. An interesting phenomenon that may also be observed occurs when a slip system intersects a grain boundary. In reality, the grain boundary acts as an impediment to dislocation motion which is expressed through the simulation as a barrier to the propagation of deformation.

SHEAR STRAIN INCREMENTS

Numerical results for the shear strain at the each active in-plane slip system, which are shown in Fig. 1, as well as total shear in aluminum bicrystal, are shown in Figure 12. Simulation results and discussion shear strains for the (110) and (001) orientations of aluminum single crystals are presented elsewhere (Chen et al., 2004 and Vukelic et al., 2006) and will not be further explained here. The orientation of crystals in the bicrystal is such that same slip systems are active and furthermore yield loci have the same shape. Due to this fact one would intuitively assume that deformation should be symmetric. However, due to the asymmetry of the domain of interest caused by the grain boundary the total shear strain is asymmetric as seen on Fig. 12d, which is consistent with the asymmetry of lattice rotation discussed in the previous section. Total shear strain indicates lobes of deformation with a higher magnitude in the right crystal where the slip direction does not point into the boundary. The explanation of this phenomenon is the same as for the lattice rotation given in the previous section. Shear strains for each active slip system are also given at Figs. 12a, b and c. Figure 12c shows that the grain boundary does not have much impact on shear strain creation in slip system ii, which is similar to shear strain on the same slip system in the reference single crystals (Chen et al, 2004, Vukelic et al, 2006). On the other hand, it can be seen that slips in slip systems i and iii experience a sharp discontinuity at the grain boundary. The portion affected by the grain boundary is the one in the sector directly under non uniform pressure loading in the reference single crystal (Vukelic et al, 2006). Discontinuity is a consequence of an inability of the slip to transmit through grain boundary as well as sudden change of resolved shear stress at the grain boundary, analogous to dislocation motion behavior mentioned in previous paragraph. Thus, plastic slip flows under compressive μLSP loading in each crystal until it reaches the grain boundary, which behaves as an obstacle to further deformation.

RESIDUAL STRESS DISTRIBUTION

Wang et al. (2005) developed analytical stress field distribution for single crystal aluminum with a $(1\bar{1}4)$ crystallographic orientation based on anisotropic slip line theory under static Gaussian pressure loading. Vukelic et al (2006) derived the solution for the (110) case and made a comparison between single crystals of (110) and $(1\bar{1}4)$ orientation under the same conditions. Numerical results for the cases

are given in references mentioned above as well. Residual stress distribution for σ_{11} stress component is given at Figure 13. From

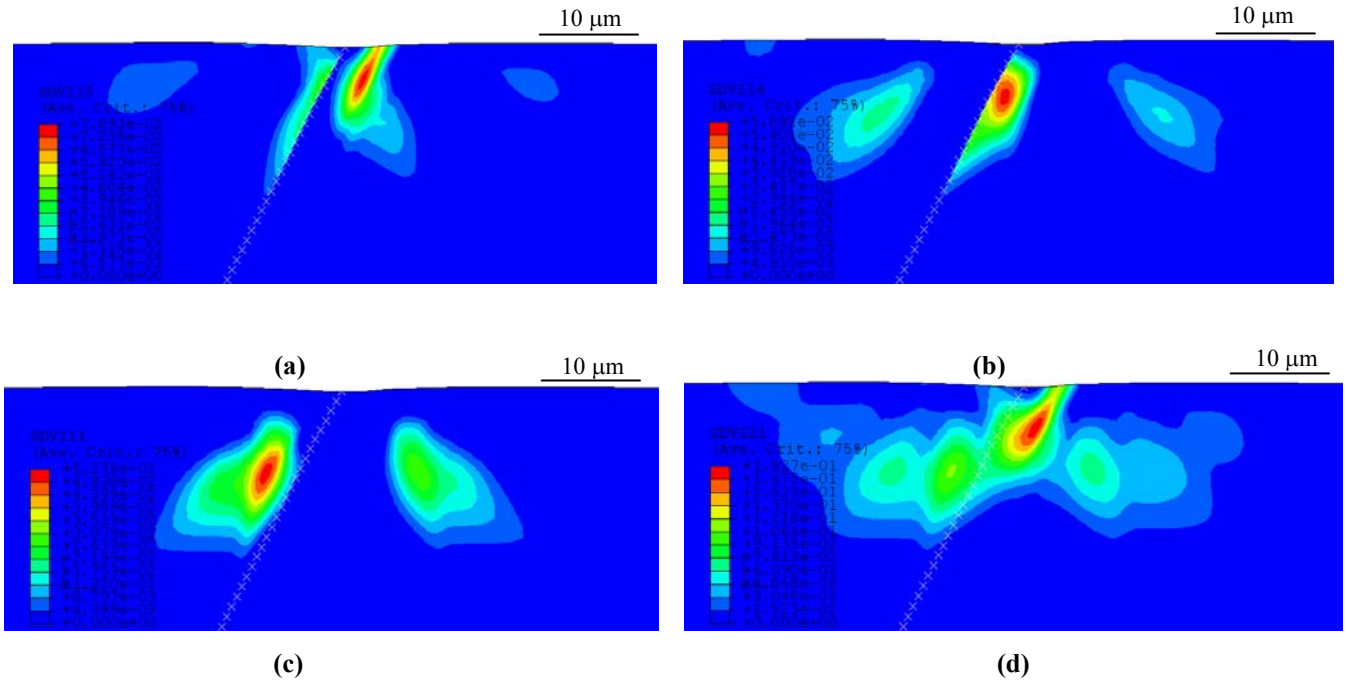

Figure 12: Numerical results – shear strain increments (a) shear strain increment iii (b) shear strain increment i (c) shear strain increment ii (d) total shear strain increment

there it can be seen that stress is continuous across grain boundary and stress field is mostly compressive and fairly symmetric. Tensile regions observed at the ends of the applied non-uniform pressure region are due to self equilibration of the stresses as discussed in detail in Wang et al (2005). The stress distribution is similar to that of the (110) single crystal case (Vukelic et al, 2006) and can be explained by the fact that both crystals in the bicrystal have symmetric yield loci resulting in the double slip case under μLSP. Small deviations from symmetry are due to the difference in angles between active slip systems and 1-1 axis for the (110) and (001) crystals.

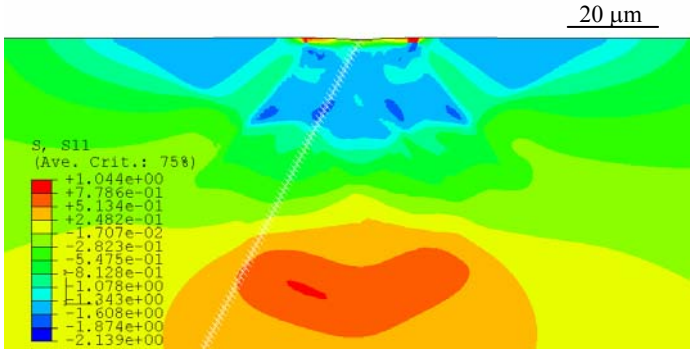

Figure 13: Residual stress distribution

CONCLUSION

The behavior of bicrystal aluminum as well as reference single crystal under Gaussian pressure loading has been presented in this study. Both, experimental and theoretical work was performed. Characterization of bicrystal and reference single crystals was done after applying μLSP and results presented. Smaller lattice rotations as well as discontinuity were observed near to the grain boundary. The numerical model based on single crystal micromechanics and cohesive zone interface model was developed and results compared with experimental findings. Numerical results have shown that under Gaussian loading potential cracks at the grain boundary tend to close and thus it can be concluded that μLSP is beneficial for expanding fatigue life of micro components under cyclic loading.

ACKNOWLEDGMENT

This work is supported under the NSF grant number: 0500239 Authors would like to thank Dr. Paul van der Wilt for his great help and assistance in acquiring EBSD data.

REFERENCES

[1] Asaro, R.J. (1983) Micromechanics of crystals and polycrystals, Advances in Applied Mechanics 23, 1-115.

[2] Asaro, R., J., Needleman, A. (1985) Texture Development and Strain Hardening in Rate Dependent Polycrystals, Acta Metallurgica, 33, 6, 923 - 953

[3] Barenblatt, G. I., (1962) Mathematical Theory of Equilibrium Cracks, Adv. Appl. Mech., 7, 56 – 129

[4] Becker, R.C. (1988) Interface Constitutive Relations for use with the Finite Element Code ABAQUS, Memorandum KZ-002, Fabricating Technology-B Group, Alcoa, Pittsburgh, Pennsylvania 15212, USA.

[5] Booker, J.R. & Davis, E.H. (1972) A general treatment of plastic anisotropy under conditions of plane strain, Journal of the Mechanics and Physics of Solids 20, 239-250.

[6] Chen, H., Yao, Y.L. & Kysar, J.W. (2004) Spatialy resolved characterization of residual stress induced by micro scale laser shock peening, ASME, Transactions Journal of Manufacturing Science and Engineering 126, 226-235.

[7] Chen, H., Yao, Y.L. & Kysar, J.W. (2004) Characterization of plastic deformation induced by microscale laser shock peening, Journal of Applied Mechanics 71, 713-723.

[8] Clauer, A.H. & Holbrook, J.H. (1981) Effects of laser induced shock waves on metals, Shock waves and high strain phenomena in metals-concepts and applications, New York, Plenum, 675-702.

[9] Clauer, A.H. & Lahrman, D.F. (2001) Laser Shock processing as a surface enhancement process, Key Engineering Materials 197, 121-142.

[10] Crone, W.C., Shield, T.W., Creuziger, A. & Henneman, B. (2004) Orientation dependence of the plastic slip near notches in ductile FCC single crystals, Journal of the Mechanics and Physics of Solids 52, 85-112.

[11] Curtis, S., de los Rios, E.R., Rodopoulos C.A., Levers A. (2002) Analysis of the effects of controlled shot peening on fatigue damage of high strength aluminium alloys, International Journal of Fatigue 25 (2003) 59–66

[12] Evers, L.P., Parks, D.M., Brekelmans, W.A.M., Geers, M.G.D. (2002) Crystal plasticity model with enhanced hardening by geometrically necessary dislocation accumulation, Journal of the Mechanics and Physics of Solids 50, 2403 – 2424

[12] Fabbro, R., Fournier, J., Ballard, P., Devaux, D. & Virmont, J. (1990) Physical study of laser-produced plasma in confined geometry, Journal of Applied Physics 68, No. 2, 775-784.

[13] Hall, E., O. (1951) The Deformation and Ageing of Mild Steel: III Discussion of Results, Proceedings Physical society B 65, 747 – 753

[14] Hertzberg, R.W. (1995) Deformation and Fracture Mechanics of Engineering, John Wiley and Sons.

[15] Hammersley, G., Hackel, L.A. & Harris, F. (2000) Surface prestressing to improve fatigue strength of components by laser shot peening, Optics and Lasers in Engineering 34, 327-337.

[16] Hill, R. (1950) The Mathematical Theory of Plasticity, Claredon Press,

[17] Hirth, J., P., Lothe, J. (1982) Theory of Dislocations, Second Edition, John Wiley & Sons

[18] Hook, R., E., Hirth, J., P. (1967) The Deformation Behavior of Isoaxial Bicrystals of Fe-3%Si, Acta Metallurgica 15, 535 – 551

[19] Huang, Y. (1991) A User-material subroutine incorporating single crystal plasticity in the ABAQUS finite element program, Mech. Report, 178, Division of Applied Sciences, Harvard University, Cambridge, MA.

[20] Kachanov, L.M. (1971) Foundations of The Theory of Plasticity, North-Holland.

[21] Kysar, J. (1997) Addendum to a user-material subroutine incorporating single crystal plasticity in the ABAQUS finite element program, Mech. Report, 178, Division of Applied Sciences, Harvard University, Cambridge, MA.

[22] Kysar, J.W. (1999) Addendum to 'Interface Constitutive Relations for use with the Finite Element Code ABAQUS', Memorandum KZ-002, Fabricating Technology-B Group, Alcoa, Pittsburgh, Pennsylvania 15212, USA

[23] Kysar, J.W. (2000) Continuumim simulations of directional dependence of crack growth along a copper/sapphire bicrystal interface. Part I: experiments and crystal plasticity background, Journal of the Mechanics and Physics of Solids 49 (2001) 1099 – 1128

[24] Kysar, J.W. & Briant, C.L. (2002) Crack tip deformation fields in

ductile single crystals, Acta Materialia 50, 2367-2380.

[25] Kysar, J.W., Gan, Y.X. & Mendez-Arzuza, G. (2005) Cylindrical void in a rigid-ideally plastic single crystal. Part I: anisotropic slip line theory solution for face-centered cubic crystals, International Journal of Plasticity 21, 1481-1520.

[26] Livingston, J. D., Chalmers, B. (1957) Multiple Slip in Bicrystal Deformation, Acta Metallurgica, 5, 322 – 327

[27] Needleman, A. (1987) A Continuum Model for Void Nucleation by Inclusion Debonding, Journal of Applied Mechanics, 54, 525 – 531

[28] Ma, A., Roters, F., Raabe, D. (2006) A dislocation density based constitutive model for crystal plasticity FEM including geometrically necessary dislocations, Acta Materialia, 54, 2169–2179

[29] Mesarevic, S., Dj., Kysar, J. W. (1996) Continuum aspects of directionally dependent cracking of an interface between copper and alumina crystals, Mechanics of Materials 23, 271-286

[30] Petch, N. J. (1953) Cleavage Strength of Polycrystals, Journal of the Iron and Steel Institute 174, 25 – 28

[31] Rey, C., Zaoui, A. (1979) Slip Heterogeneities in Deformed Aluminum Bicrystals, Acta Metallurgica, 28, 687 – 697

[31] Rice, J.R. (1973) Plane strain slip line theory for anisotropic rigid/plastic materials, Journal of the Mechanics and Physics of Solids 21, 63 -74.

[32] Rice, J.R. (1987) Tensile crack tip fields in elastic-ideally plastic crystals, Mechanics of Materials 6, 317-335.

[33] Vukelic, S., Wang, Y., Kysar, J.,W., Yao, Y., L. (2006) Comparative Study of Symmetric and Asymmetric Deformation of Al Single Crystal Under Micro Scale Shock Peening, Submitted

[34] Wang, Y., Kysar, J.W. & Yao, Y.L. (2005) Analytical solution of anisotropic plastic deformation induced by micro-scale laser shock peening, Submitted.

[35] Wei, Y. J., Anand, L. (2004) Grain-boundary sliding and separation in polycrystalline metals: application to nanocrystalline fcc metals, Journal of the Mechanics and Physics of Solids 52, 2587–2616

[36] Xu, X. P. and Needleman, A., (1993), Void nucleation by inclusion debonding in a crystal matrix, Modelling Simul. Mater. Sci. Eng. 1, 111-132.

[37] Xu, X. P. and Needleman, A. (1994), Numerical Simulations of Fast Crack Growth in Brittle Solids, J. Mech. Phys. Solids, 42, No. 9, 1397-1434,

[38] Zaefferer, S.,. Kuo, J.-C, Zhao, Z., Winning, M., Raabe, D. (2003) On the Influence of the Grain boundary Misorientation on the Plastic Deformation of Aluminum Bicrystals, Acta Materialia 51, 4719-4735.

[39] Zhang, W. & Yao, Y.L. (2002) Microscale laser shock processing of metallic components, Journal of Solar Energy Engineering, Transactions of the ASME, 124, 369-378.

